Louisiana State University

Craft and Hawkins Department of Petroleum Engineering

Numerical Methods in Reservoir Simulation

PETE 7280 Final Project

Esmail Ansari

December 2013

Abstract

The numerical simulation of a 2D two-phase and a 3D two—phase reservoir consisting of water and oil is carried out. The simulator is validated with Buckley-Leverette analytical solution of the two-phase flow equations. A 2D reservoir and a similar 3D reservoir are considered for simulation. Attained results of the 3D case is compared and validated with the results of CMG software. Two pressure transient methods, drawdown and buildup, are used for calculating the permeability of the reservoir based on synthetic flow data from the simulator. A sensitivity analysis on the effect of various parameters on the accuracy of the calculated permeability is performed and the results are analyzed.

Table of Contents

Table of Figures

1 Buckley-Leverett study

1.1 Formulation of fractional flow equation

Starting from the Darcy's equations, we have:

$$q_o = -\frac{kk_{ro}A}{\mu_o}\left(\frac{\partial P_o}{\partial x} + \rho_o g sin(\alpha)\right) \quad \text{Eq. 1}$$

$$q_w = -\frac{kk_{rw}A}{\mu_w}\left(\frac{\partial P_w}{\partial x} + \rho_w g sin(\alpha)\right) \quad \text{Eq. 2}$$

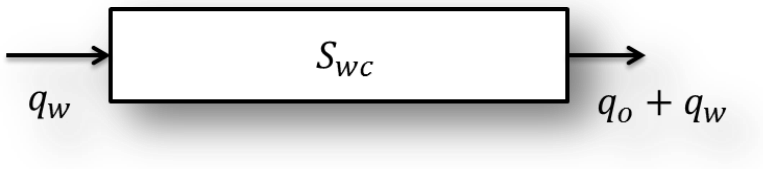

Figure 1: Displacement of oil by water

By substituting the $P_w = P_o - P_{cow}$, and subtracting oil and water Darcy's equation, we have:

$$-\frac{1}{kA}\left(q_w\frac{\mu_w}{k_{rw}} - q_o\frac{\mu_o}{k_{ro}}\right) = -\frac{\partial P_{cow}}{\partial x} + \Delta\rho g \sin(\alpha) \quad \text{Eq. 3}$$

and substituting for $q = q_w + q_o \; and \; f_w = \frac{q_w}{q}$, we get:

$$f_w = \frac{\left(1 + \frac{kk_{ro}A}{q\mu_o}\left(\frac{\partial P_{cow}}{\partial x} - \Delta\rho g sin(\alpha)\right)\right)}{1 + \frac{k_{ro}}{\mu_o}\frac{\mu_w}{k_{rw}}} \quad \text{Eq. 4}$$

For a simple horizontal flow, with negligible capillary, the fractional flow expression reduces to:

$$f_w = \frac{1}{1 + \frac{k_{ro}}{\mu_o}\frac{\mu_w}{k_{rw}}} \qquad \text{Eq. 5}$$

which shows that fractional flow is controlled by relative permeability. If we assume that water and oil viscosity are known, the fractional flow is only function of water saturation: $f_w = f_w(S_w)$.

1.2 Formulation of the Buckley-Leverett equation

From the continuity equation for two-phase flow in single dimension we have:

$$-\frac{\partial(q_w \rho_w)}{\partial x} = \frac{A\phi\partial(S_w \rho_w)}{\partial t} \qquad \text{Eq. 6}$$

In this equation, if we assume that ρ_w is constant, $q_w = f_w q$ and also knowing from the previous section that $f_w = f_w(S_w)$, the equation can be written as:

$$-\frac{df_w}{dS_w}\frac{\partial S_w}{\partial x} = \left(\frac{A\phi}{q}\frac{\partial S_w}{\partial t}\right) \qquad \text{Eq. 7}$$

This equation is known as Buckley-Leverett equation.

1.3 Formulation of frontal advance equation

We know that $S_w = S_w(x, t)$, so following expression can be written using chain rule:

$$dS_w = \frac{\partial S_w}{\partial x}dx + \frac{\partial S_w}{\partial t}dt \qquad \text{Eq. 8}$$

Buckley leveret solution follows the fluid front of each saturation during displacement, so we assume that $dS_w = 0$, to come up with a formulation for each saturation front movement:

$$0 = \frac{\partial S_w}{\partial x} dx + \frac{\partial S_w}{\partial t} dt \qquad \text{Eq. 9}$$

Substituting into the Buckley-Leverett equation developed in previous section, we get:

$$\frac{dx}{dt} = \frac{q}{A\phi} \frac{df_w}{dS_w} \qquad \text{Eq. 10}$$

An integration of this equation in time yields:

$$x_f = \frac{qt}{A\phi} \left(\frac{df_w}{dS_w} \right) \qquad \text{Eq. 11}$$

which is known as the frontal advance equation. We further make Eq. 11 dimensionless by defining following variables:

$$x_D = \frac{x}{L} \qquad \text{Eq. 12}$$

$$t_D = \frac{q_t t}{A\phi L} \qquad \text{Eq. 13}$$

$$f'_{wf} = \frac{f_{wf} - f_{iw}}{S_{wf} - S_{iw}} \qquad \text{Eq. 14}$$

in which $f_{wf}{}'$ represents the slope from the connate water point to the fractional flow curve. This substitution results in:

$$x_{DSw} = f_w{}' t_D \qquad \text{Eq. 15}$$

1.4 Formulation of relative permeability equation

Corey relative permeability equation is used for calculating relative permeability of the reservoir. This equation is developed experimentally.

$$k_{ro}(S_w) = k_{ro}^0 \left(\frac{1 - S_w - S_{or}}{1 - S_{wr} - S_{or}}\right)^a \quad \text{Eq. 16}$$

$$k_{rw}(S_w) = k_{rw}^0 \left(\frac{S_w - S_{wr}}{1 - S_{wr} - S_{or}}\right)^b \quad \text{Eq. 17}$$

We use below parameters in the above equations for both our simulator and solving Buckley-Leverett equations and plot the relative permeability curve (Figure 2) which shows that the rock is intermediate (neither water wet or oil wet):

$$S_{wr} = 0.2, \quad S_{or} = 0.2, \quad k_{rw}^0 = 1\,, \quad k_{ro}^0 = 1 \quad \text{Eq. 18}$$
$$a = 2\,, b = 2$$

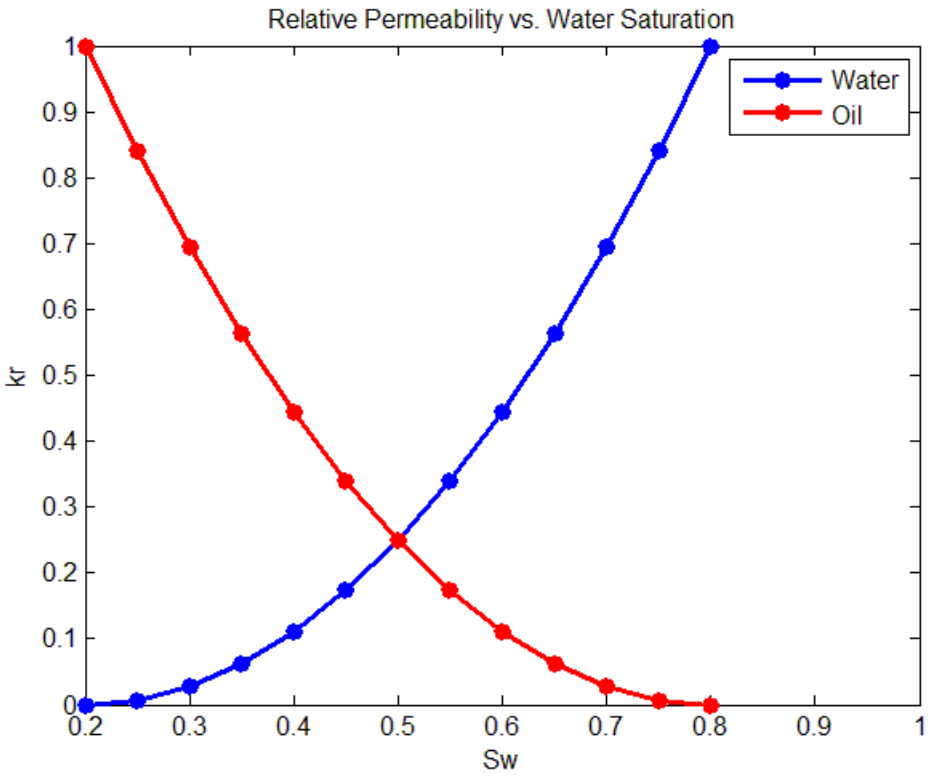

Figure 2: Corey equation for calculating relative permeability.

1.5 Solution to the analytical equations

For solving Buckley-Leverett equation, we know that fractional flow equation is a function of relative permeability and relative permeability is a function of saturation. Hence we find the saturation that has the maximum speed by using the tangential line (Eq. 14). This saturation is the saturation of the advancing front after which we have connate water. Before this front, the derivative of the fractional flow is used in Eq. 15 to calculate the S_w profile.

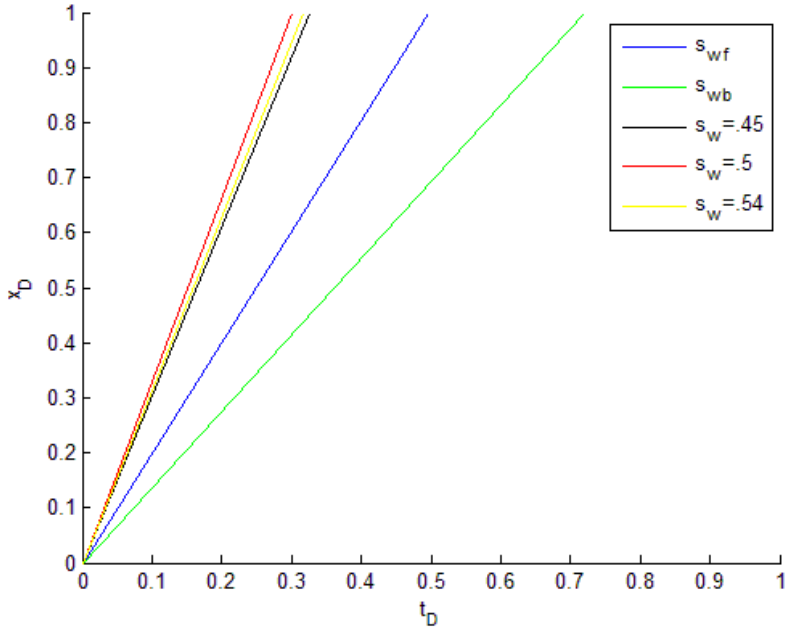

Figure 3: Derivative of the fractional flow curve at different S_w

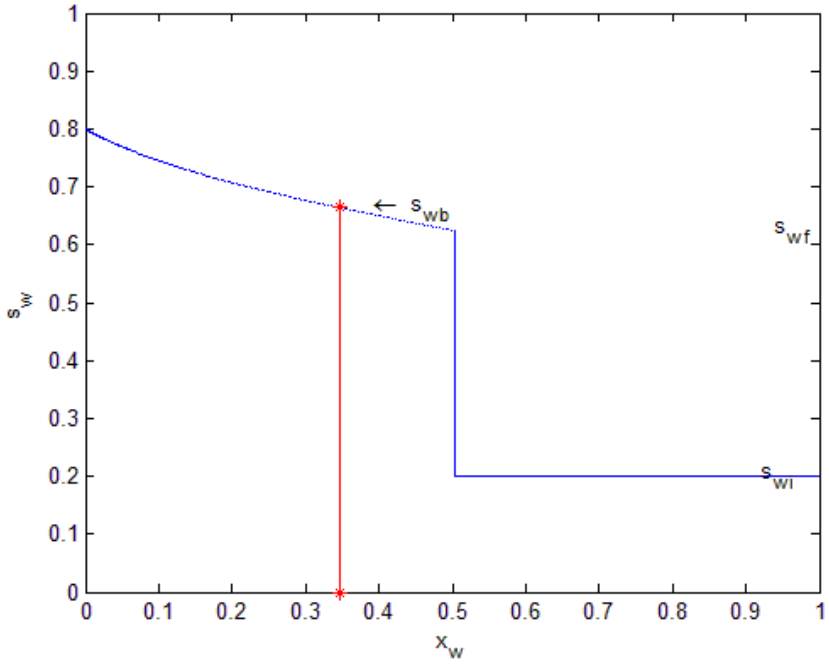

Figure 4: Advancing front at $t_D = 0.25$

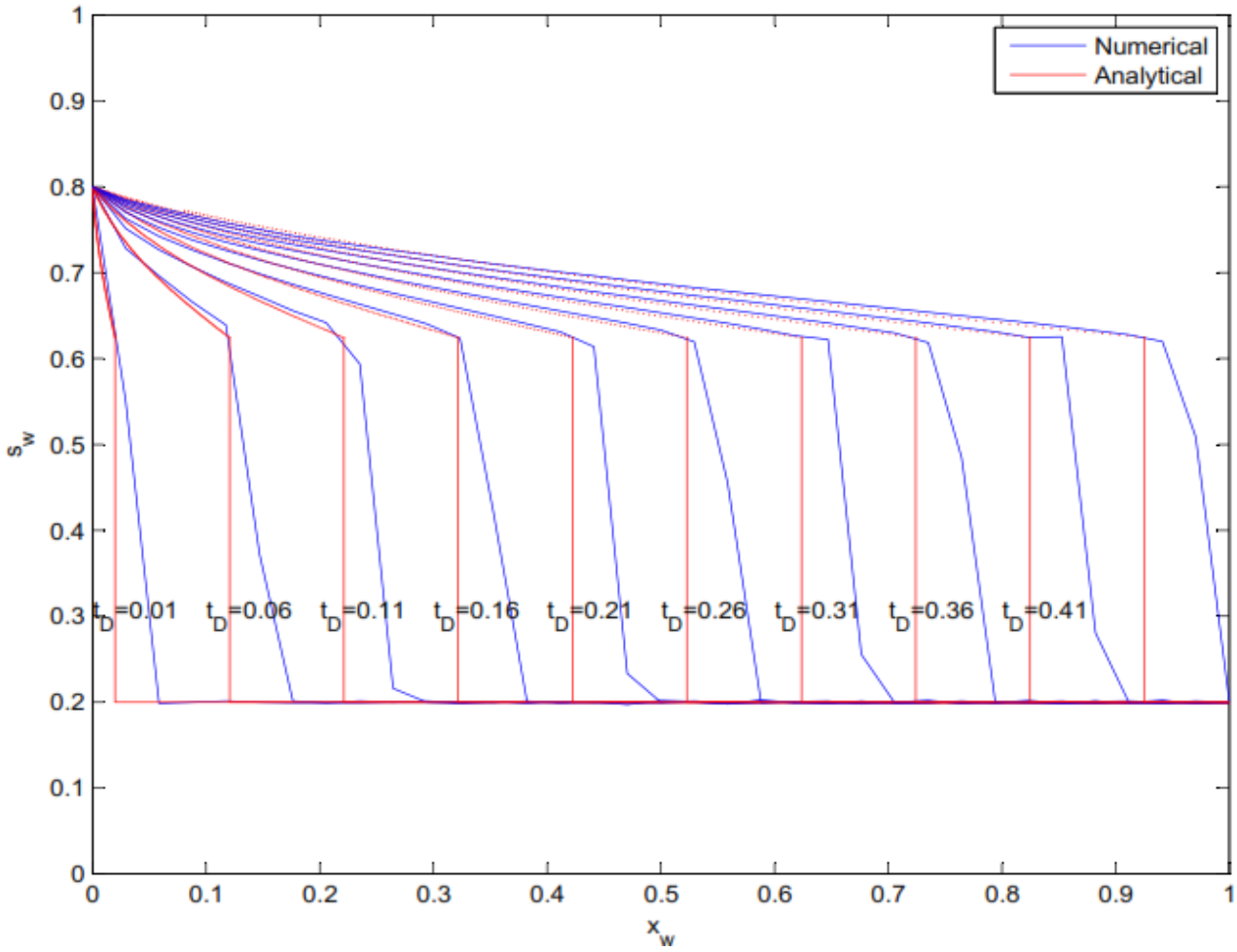

Figure 5: Validation of the simulator with Buckley-Leverett analytical solution

2 A two-dimensional two-phase case

2.1 2D IMPES approach

Two dimensional IMPES is very similar to one dimensional IMPES. The only difference is that there exist another direction for y and as a result we have two kind of Transmissibility; one in the x direction and one in y direction.

The general formulas for having two phase flow in two dimensions are summarized below:

$$-\frac{\partial}{\partial x}\left(u_l\rho_l\right)-\frac{\partial}{\partial y}\left(u_l\rho_l\right)=\frac{\partial}{\partial t}\left(\phi\rho_l S_l\right) \qquad l=o,w \qquad \text{Eq. 19}$$

$$u_l=-\frac{kk_{rl}}{\mu_l}\frac{\partial P_l}{\partial x} \quad l=o,w \qquad \text{Eq. 20}$$

$$u_l=-\frac{kk_{rl}}{\mu_l}\frac{\partial P_l}{\partial y} \quad l=o,w \qquad \text{Eq. 21}$$

$$P_{cow}=P_o-P_w \qquad \text{Eq. 22}$$

$$\sum_{l=o,w} S_l=1$$

Substituting Darcy equations into the continuity equations yields:

$$\frac{\partial}{\partial x}\left(\frac{kk_{ro}}{\mu_o B_o}\frac{\partial P_o}{\partial x}\right)+\frac{\partial}{\partial y}\left(\frac{kk_{ro}}{\mu_o B_o}\frac{\partial P_o}{\partial y}\right)-q_o'=\frac{\partial}{\partial t}\left(\frac{\phi S_o}{B_o}\right) \qquad \text{Eq. 23}$$

$$\frac{\partial}{\partial x}\left(\frac{kk_{rw}}{\mu_w B_w}\frac{\partial P_o}{\partial x}\right)+\frac{\partial}{\partial y}\left(\frac{kk_{rw}}{\mu_w B_w}\frac{\partial P_o}{\partial y}\right)-q_w'=\frac{\partial}{\partial t}\left(\frac{\phi S_w}{B_w}\right) \qquad \text{Eq. 24}$$

$$P_{cow}=P_o-P_w \qquad \text{Eq. 25}$$

$$S_0+S_w=1 \qquad \text{Eq. 26}$$

Discretization of the first part of above equations gives:

$$\frac{\partial}{\partial x}\left(\frac{kk_{ro}}{\mu_o B_o}\frac{\partial P_o}{\partial x}\right)_{i,j}+\frac{\partial}{\partial y}\left(\frac{kk_{ro}}{\mu_o B_o}\frac{\partial P_o}{\partial y}\right)_{i,j}=T_{xo_{i+1/2,j}}\left(P_{o_{i+1,j}}-P_{o_{i,j}}\right)-T_{xo_{i-1/2,j}}\left(P_{o_{i,j}}-P_{o_{i-1,j}}\right)+ T_{yo_{i,j+1/2}}\left(P_{o_{i,j+1}}-P_{o_{i,j}}\right)-T_{yo_{i,j-1/2}}\left(P_{o_{i,j}}-P_{o_{i,j-1}}\right) \quad \text{Eq. 27}$$

$$\frac{\partial}{\partial x}\left(\frac{kk_{rw}}{\mu_w B_w}\frac{\partial P_w}{\partial x}\right)_{i,j}+\frac{\partial}{\partial y}\left(\frac{kk_{rw}}{\mu_w B_w}\frac{\partial P_w}{\partial y}\right)_{i,j}=T_{xw_{i+1/2,j}}\left(P_{w_{i+1,j}}-P_{w_{i,j}}\right)-T_{xw_{i-1/2,j}}\left(P_{w_{i,j}}-P_{w_{i-1,j}}\right)+ T_{yo_{i,j+1/2}}\left(P_{w_{i,j+1}}-P_{w_{i,j}}\right)-T_{yw_{i,j-1/2}}\left(P_{w_{i,j}}-P_{w_{i,j-1}}\right) \quad \text{Eq. 28}$$

The transmissibility can be regarded as having two directions, one in the x and the other in the y direction:

$$T_{xo_{i+1/2,j}}=\frac{2\lambda_{o_{i+1/2,j}}}{\Delta x_{i,j}\left(\frac{\Delta x_{i,j}}{k_{i,j}}+\frac{\Delta x_{i+1,j}}{k_{i+1,j}}\right)} \quad \text{Eq. 29}$$

$$T_{xw_{i+1/2,j}}=\frac{2\lambda_{w_{i+1/2,j}}}{\Delta x_{i,j}\left(\frac{\Delta x_{i,j}}{k_{i,j}}+\frac{\Delta x_{i+1,j}}{k_{i+1,j}}\right)} \quad \text{Eq. 30}$$

$$T_{yo_{i,j+1/2}}=\frac{2\lambda_{o_{i,j+1/2}}}{\Delta y_{i,j}\left(\frac{\Delta y_{i,j}}{k_{i,j}}+\frac{\Delta y_{i,j+1}}{k_{i,j+1}}\right)} \quad \text{Eq. 31}$$

$$T_{yw_{i,j+1/2}}=\frac{2\lambda_{w_{i,j+1/2}}}{\Delta y_{i,j}\left(\frac{\Delta y_{i,j}}{k_{i,j}}+\frac{\Delta y_{i,j+1}}{k_{i,j+1}}\right)} \quad \text{Eq. 32}$$

$$\lambda_o=\frac{k_{ro}}{\mu_o B_o} \quad \text{Eq. 33}$$

$$\lambda_w=\frac{k_{rw}}{\mu_w B_w} \quad \text{Eq. 34}$$

It is recommended to use upstream flow in the programming to get a better result that is more realistic:

$$\lambda_{o_{i+1/2,j}} = \begin{cases} \lambda_{o_{i+1,j}} & if \quad P_{o_{i+1,j}} \geq P_{o_{i,j}} \\ \lambda_{o_{i,j}} & if \quad P_{o_{i+1,j}} < P_{o_{i,j}} \end{cases} \qquad \text{Eq. 35}$$

$$\lambda_{w_{i+1/2,j}} = \begin{cases} \lambda_{w_{i+1,j}} & if \quad P_{w_{i+1,j}} \geq P_{w_{i,j}} \\ \lambda_{w_{i,j}} & if \quad P_{w_{i+1,j}} < P_{w_{i,j}} \end{cases}$$

$$\lambda_{o_{i,j+1/2}} = \begin{cases} \lambda_{o_{i,j+1}} & if \quad P_{oi,j+1} \geq P_{o_{i,j}} \\ \lambda_{o_{i,j}} & if \quad P_{o_{i,j+1}} < P_{o_{i,j}} \end{cases} \qquad \text{Eq. 36}$$

$$\lambda_{w_{i,j+1/2}} = \begin{cases} \lambda_{wi,j+1} & if \quad P_{wi,j+1} \geq P_{w_{i,j}} \\ \lambda_{w_{i,j}} & if \quad P_{w_{i,j+1}} < P_{w_{i,j}} \end{cases}$$

Used coefficient for discretizing the right hand side of the general equations are listed below:

$$C_{poo_{i,j}} = \frac{\phi_{i,j}\left(1-S_{w_{i,j}}\right)}{\Delta t}\left[\frac{c_r}{B_o} + \frac{d\left(1/B_o\right)}{dP_o}\right]_{i,j} \qquad \text{Eq. 37}$$

$$C_{swo_{i,j}} = -\frac{\phi_{i,j}}{B_{o_{i,j}}\Delta t}$$

$$C_{pow_{i,j}} = \frac{\phi_{i,j}S_{w_{i,j}}}{\Delta t}\left[\frac{c_r}{B_w} + \frac{d\left(1/B_w\right)}{dP_w}\right]_{i,j}$$

$$C_{sww_{i,j}} = \frac{\phi_{i,j}}{B_{w_{i,j}}\Delta t} - \left(\frac{\partial P_{cow}}{\partial S_w}\right)_{i,j} C_{pow_{i,j}}$$

For this case the we have assumed that Bw and Bo are constant and don't change with pressure. We discussed it in the assumptions. However the capillary pressure change with saturation is calculated using numerical derivative methods, and then spline interpolation is used on the results. If we combine the attained discretized equations altogether we have:

$$T_{xo\,i+1/2,j}^{\ t}\left(P_{o_{i+1,j}}-P_{oi,j}\right)+T_{xo\,i-1/2,j}^{\ t}\left(P_{o_{i-1,j}}-P_{oi,j}\right)+T_{yo\,i,j+1/2}^{\ t}\left(P_{o_{i,j+1}}-P_{oi,j}\right)+T_{yo\,i,j-1/2}^{\ t}\left(P_{o_{i,j-1}}-P_{oi,j}\right)-q'_{oi,j}$$
$$=C_{pooi,j}^{\ t}\left(P_{o_{i,j}}-P_{o\,i,j}^{\ t}\right)+C_{swoi,j}^{\ t}\left(S_{w_{i,j}}-S_{wi,j}^{\ t}\right)\qquad i=1,....,N \qquad \text{Eq. 38}$$

$$T_{xw\,i+1/2,j}^{\ t}\left[\left(P_{o_{i+1,j}}-P_{oi,j}\right)-\left(P_{cow_{i+1,j}}-P_{cow_{i,j}}\right)^{t}\right]+T_{xw\,i-1/2,j}^{\ t}\left[\left(P_{o_{i-1,j}}-P_{oi,j}\right)-\left(P_{cow_{i-1,j}}-P_{cow_{i,j}}\right)^{t}\right]$$
$$T_{yw\,i,j+1/2}^{\ t}\left[\left(P_{o_{i,j+1}}-P_{oi,j}\right)-\left(P_{cow_{i,j+!}}-P_{cow_{i,j}}\right)^{t}\right]+T_{yw\,i,j-1/2}^{\ t}\left[\left(P_{o_{i,j-1}}-P_{oi,j}\right)-\left(P_{cow_{i,j-1}}-P_{cow_{i,j}}\right)^{t}\right]-q'_{wi,j} \qquad \text{Eq. 39}$$
$$=C_{powi}^{\ t}\left(P_{o_{i,j}}-P_{oi,j}^{\ t}\right)+C_{swwi}^{\ t}\left(S_{w_{i,j}}-S_{wi,j}^{\ t}\right)\qquad i=1,....,N$$

Multiplying the first equation by a factor and then summing these equations and eliminating the water saturation yields:

$$\left(T_{xo\,i+1/2,j}^{\ t}+\alpha_i T_{xw\,i+1/2,j}^{\ t}\right)\left(P_{o_{i+1,j}}-P_{oi,j}\right)+\left(T_{xo\,i-1/2,j}^{\ t}+\alpha_i T_{xw\,i-1/2,j}^{\ t}\right)\left(P_{o_{i-1,j}}-P_{oi,j}\right)$$
$$-\alpha_{i,j}T_{xw\,i+1/2,j}^{\ t}\left(P_{cow_{i+1,j}}-P_{cow_{i,j}}\right)^{t}-\alpha_i T_{xw\,i-1/2,j}^{\ t}\left(P_{cow_{i-1,j}}-P_{cow_{i,j}}\right)^{t}$$
$$+\left(T_{yo\,i,j+1/2}^{\ t}+\alpha_i T_{yw\,i,j+1/2}^{\ t}\right)\left(P_{o_{i,j+1}}-P_{oi,j}\right)+\left(T_{yo\,i,j-1/2}^{\ t}+\alpha_i T_{yw\,i,j-1/2}^{\ t}\right)\left(P_{o_{i-1,j}}-P_{oi,j}\right)$$
$$-\alpha_{i,j}T_{yw\,i,j+1/2}^{\ t}\left(P_{cow_{i,j+1}}-P_{cow_{i,j}}\right)^{t}-\alpha_i T_{yw\,i,j-1/2}^{\ t}\left(P_{cow_{i,j-1}}-P_{cow_{i,j}}\right)^{t}$$
$$-q'_{oi,j}-\alpha_i q'_{wi,j}=\left(C_{pooi,j}^{\ t}+\alpha_{i,j}C_{powi,j}^{\ t}\right)\left(P_{o_{i,j}}-P_{o\,i,j}^{\ t}\right)\qquad i=1,....,N\quad j=1,....,N$$
Eq. 40

However, above equations is too complicated to be used, thus it is more suitable to

$$\alpha_{i,j}=-C_{swoi,j}^{\ t}/C_{swwi,j}^{\ t} \qquad \text{Eq. 41}$$

arrange it.

$$W_{i,j}P_{o_{i-1,j}}+S_{i,j}P_{o_{i,j-1}}+M_{i,j}P_{oi,j}+N_{i,j}P_{o_{i,j+1}}+E_{i,j}P_{o_{i+1,j}}=d_{i,j}\qquad i=1,....,N\quad j=1,....,N \qquad \text{Eq. 42}$$

$$W_{i,j} = T_{xo}{}^{t}_{i-1/2,j} + \alpha_{i,j} T_{xw}{}^{t}_{i-1/2}$$

$$S_{i,j} = T_{yo}{}^{t}_{i,j-1/2} + \alpha_{i,j} T_{yw}{}^{t}_{i,j-1/2}$$

$$E_{i,j} = T_{xo}{}^{t}_{i+1/2,j} + \alpha_{i,j} T_{xw}{}^{t}_{i+1/2,j}$$

$$N_{i,j} = T_{yo}{}^{t}_{i,j+1/2} + \alpha_{i,j} T_{yw}{}^{t}_{i,j+1/2}$$

$$M_{i,j} = -\left(T_{xo}{}^{t}_{i+1/2,j} + T_{xo}{}^{t}_{i-1/2,j} + T_{yo}{}^{t}_{i,j+1/2} + T_{yo}{}^{t}_{i,j-1/2} + C_{pooi,j}^{t}\right) - \alpha_{i,j}\left(T_{xw}{}^{t}_{i+1/2,j} + T_{xw}{}^{t}_{i-1/2,j} + T_{yw}{}^{t}_{i,j+1/2} + T_{yw}{}^{t}_{i,j-1/2} + C_{powi,j}^{t}\right)$$

$$b_{i,j} = -\left(C_{pooi,j}^{t} + \alpha_{i,j} C_{powi,j}^{t}\right) P_{o_{i,j}}^{t} + q'_{oi,j} + \alpha_{i,j} q'_{wi,j} + \alpha_{i,j} T_{xw}{}^{t}_{i+1/2,j}\left(P_{cow_{i+1,j}} - P_{cow_{i,j}}\right)^{t} + \alpha_{i,j} T_{xw}{}^{t}_{i-1/2,j}\left(P_{cow_{i-1,j}} - P_{cow_{i,j}}\right)^{t}$$
$$+\alpha_{i,j} T_{yw}{}^{t}_{i,j+1/2}\left(P_{cow_{i,j+1}} - P_{cow_{i,j}}\right)^{t} + \alpha_{i,j} T_{yw}{}^{t}_{i,j-1/2}\left(P_{cow_{i,j-1}} - P_{cow_{i,j}}\right)^{t}$$

Eq. 43

After solving the above equations and calculating the pressure, the saturation of each cell can be calculated explicitly.

$$S_{w_{i,j}} = S_{wi,j}^{t} + \frac{1}{C_{swoi,j}^{t}}\left[\begin{array}{l} T_{xo}{}^{t}_{i+1/2,j}\left(P_{o_{i+1,j}} - P_{oi,j}\right) + T_{xo}{}^{t}_{i-1/2,j}\left(P_{o_{i-1,j}} - P_{oi,j}\right) + \\ T_{yo}{}^{t}_{i,j+1/2}\left(P_{o_{i,j+1}} - P_{oi,j}\right) + T_{yo}{}^{t}_{i,j-1/2}\left(P_{o_{i,j-1}} - P_{oi,j}\right) - q'_{oi,j} - C_{pooi,j}^{t}\left(P_{o_{i,j}} - P_{oi,j}^{t}\right) \end{array}\right] \begin{array}{l} i = 1,....,N \\ j = 1,....,N \end{array}$$

Eq. 44

For the grids that have production with constant pressure like our case the above equation is changed to the below equation:

$$S_{w_{i,j}} = S_{wi,j}^{t} + \frac{1}{C_{swoi,j}^{t}}\left[\begin{array}{l} T_{xo}{}^{t}_{i+1/2,j}\left(P_{o_{i+1,j}} - P_{oi,j}\right) + T_{xo}{}^{t}_{i-1/2,j}\left(P_{o_{i-1,j}} - P_{oi,j}\right) + \\ T_{yo}{}^{t}_{i,j+1/2}\left(P_{o_{i,j+1}} - P_{oi,j}\right) + T_{yo}{}^{t}_{i,j-1/2}\left(P_{o_{i,j-1}} - P_{oi,j}\right) - \dfrac{WC_i}{A\Delta x_i}\lambda_{oi}^{t} P_{bh_i} - C_{pooi,j}^{t}\left(P_{o_{i,j}} - P_{oi,j}^{t}\right) \end{array}\right] \begin{array}{l} i = 1,....,N \\ j = 1,....,N \end{array}$$

Eq. 45

$$r_e = \sqrt{\frac{\Delta y \Delta x_i}{\pi}} \qquad \text{Eq. 46}$$

$$WC_i = \frac{2\pi k_i h}{\ln\left(r_e / r_w\right)} \qquad \text{Eq. 47}$$

2.2 Grid Arrangement

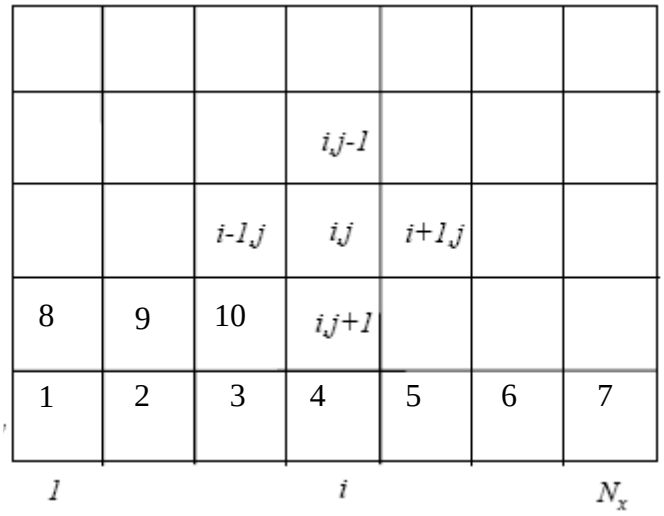

Figure 6: Arrangement of the grids

The above arrangement shows the method used for solving this homework, note that the number of the grid is in relation to i and j:

$$m = I + (j-1) * Nx \qquad \text{Eq. 48}$$

The obtained equations for the pressure will be arranged into following manner:

Figure 7: Arrangement of solving matrix (pressure)

2.3 Reservoir Description

A five spot water flooding pattern is considered in which the injector is located at the center of a two dimensional cube. The model is assumed to be homogenous and symmetric and the results of only one of the wells are presented below. No-flow condition is considered on the peripheral boundaries of the reservoir. The permeability of the reservoir is considered to be 10 md and the porosity of the reservoir is 0.3. We inject water at the center of the reservoir with a rate of $200\ bbl/day$ and set the production well bottom hole pressure to $2500\ psi$. The properties of the reservoir are summarized in below tables. The simulation stops when one of the wells reaches water cut of more than 0.95 percent.

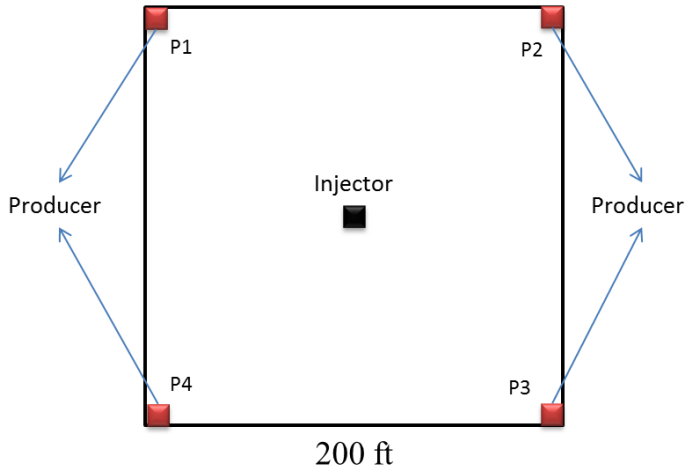

Figure 8: Schematic of the considered five spot problems

Reservoir water saturation	Reservoir height	Reservoir width	Reservoir Length	Initial reservoir pressure
0.25	30 ft	200 ft	200 ft	3000 psi

Oil Viscosity	Water Viscosity
3 cp	1 cp

Compressibility factor	Production well pressure	water injection rate
$45e-6\ \frac{1}{psi}$	2500 psi	200 bbl/day

2.4 Assumptions

1. The formation volume factor of both oil and water are assumed to be constant.
2. The viscosity of both water and oil is considered to be constant.

3. The reservoir is initially filled with oil so the initial Sw is 0.25.
4. The radius of the wells is set to 0.33.
5. No flow boundary condition is assumed.

2.5 Unit Selection

The units are set to field units and are based on the following equation.

$$q * 5.615 = 1.127 * 10^{-3} \frac{k}{\mu} \frac{A}{B_o} \frac{\partial p}{\partial r} \qquad \text{Eq. 49}$$

with P in psi, r in ft, Ct in psi-1, k in md and μ in cp and q in STB/day.

Using these units the unit of both sides will be 1/day. This requires multiplying the mobility by a factor of (1.127e-3/5.615) and then we can use field units for the IMPES method. Water saturation distribution

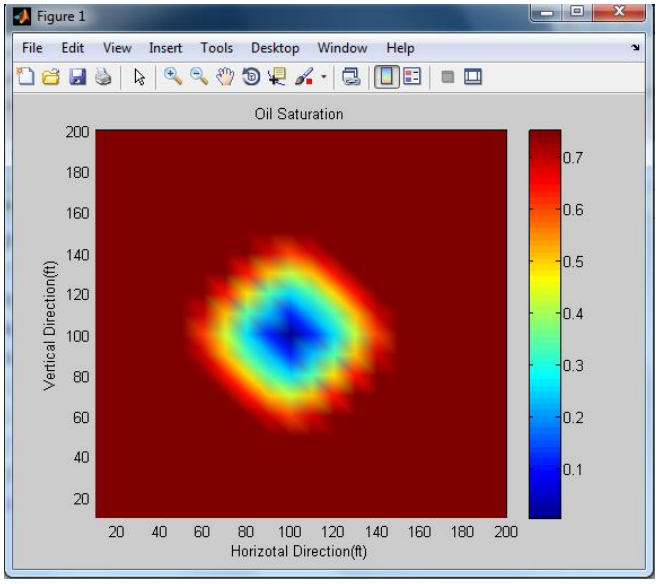

Figure 9: Water saturation distribution after 10 days. As soon as water injection begins the saturation around injecting cell rises form the value of 0.25.

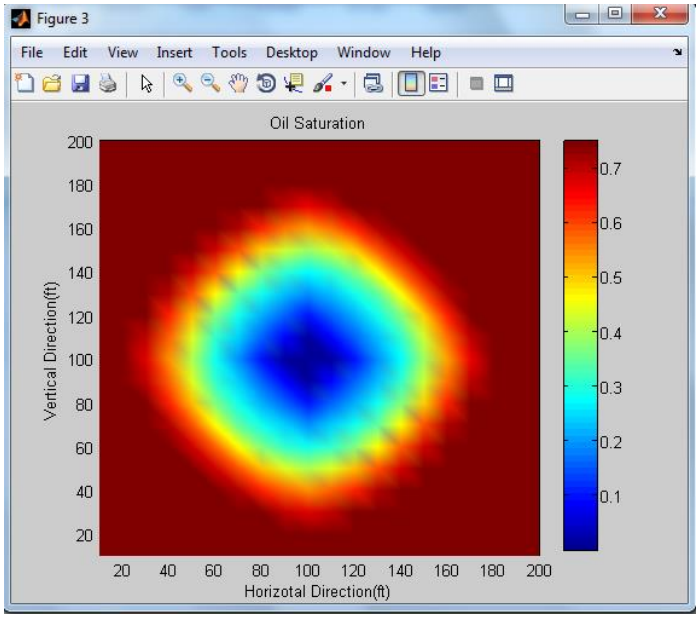

Figure 10: Water saturation distribution after 30 days. The advancement of the front and decrease in oil saturation is illustrated in this figure. The reduction in speed of the water

saturation advancement is associated with two factors: first that constant injection rate has to disperse between a larger area and second that the pressure gradient decreases.

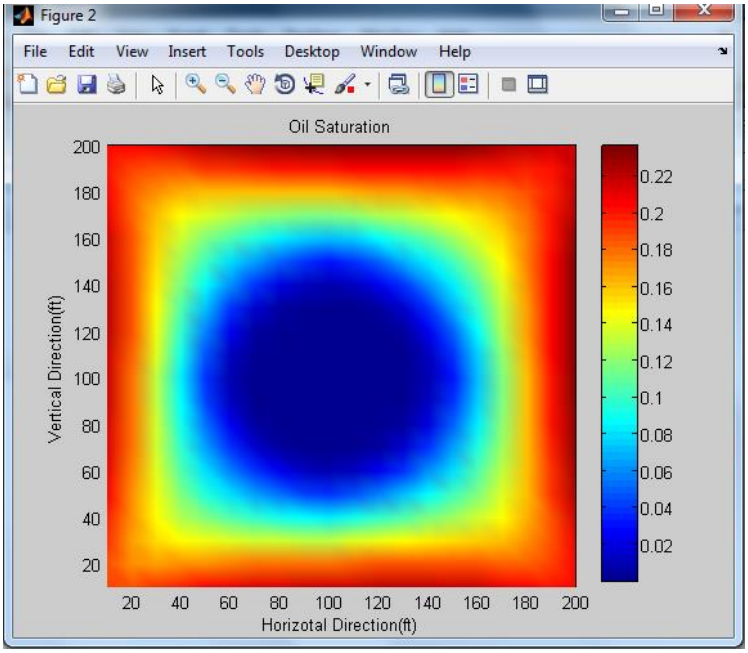

Figure 11: Water saturation distribution after 95% water cut for well number 1. As the pressure of the reservoir increases, the speed of saturation advancement falls down. This is because the primary pushing force for water saturation is pressure gradient.

2.6 Results

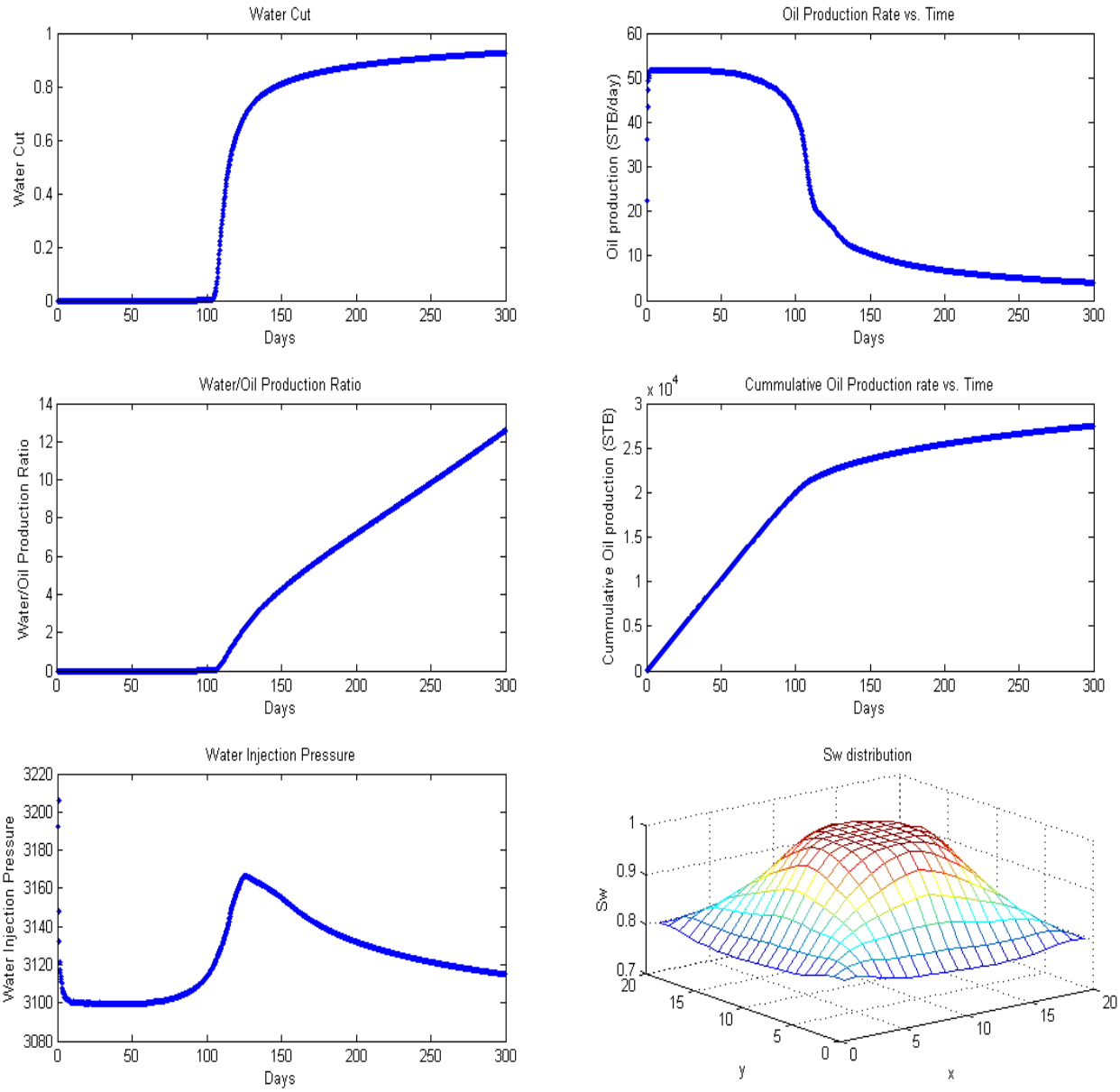

Figure 12: Various Plots for one of the wells after 95% water cut.

2.7 Discussing the results

Before explaining the above figures, we must note that we have two different pressures; the first is injecting pressure which associates to the injector and the second is the

injecting cell pressure which relates to the reservoir sand face and is independent of injector pressure. These two pressures are correlated to each other through injecting rate.

From Figure 12, we can see that rate of injection and production is not the same. The reason is that the producer works at constant pressure not at constant rate. If the production was at constant rate, such a phenomenon would have occurred. As soon as breakthrough occurs, the oil saturation around the production cells decreases, therefore we can see that oil production rapidly decreases.

Since the rate of injection is remained constant, the injection pressure depends only on mobility, W_{ci} and the injecting grid size. The mobility is dependent on absolute and relative permeability as well as viscosity. At the beginning the reservoir has S_w of 0.25 and its relative permeability is very low which causes its transmissibility to be low; therefore we expect the pressure to go up in the cell and because of that, we need decreasing water injection pressure which makes sense. But why does after some time the pressure of injector increase? This phenomenon starts with breakthrough. If the water injection continues, the water saturation has to scatter in a larger area with a very low mobility ratio corresponding to the initial water saturation of 0.25. The drop in the pressure gradient in the reservoir requires more pushing force for the same rate of injection into the sand face. Because all the forces of water advancement like imbibition and pressure gradient drops as soon as water disperses in larger area of the reservoir. The increase in the water production and water oil ratio as well as decrease in the slope of cumulative oil are the consequences of this scattering of water flooding front.

The reason for decreasing bottom hole pressure at the last interval is that at last stage the saturation of water in the entire reservoir is high and therefore the mobility of water is high; we need less injection pressure for pushing the saturation forward. The difference between the third and the second stages is that in the second region (which was discussed in the previous question) the breakthrough makes the water saturation of the producer's adjacent cells to remain low so more thrusting force is needed for pushing water forward however in the third region the saturation of water in the reservoir is so high that such force does not even needed.

But why does the rate of oil production first increase and then decrease? Why doesn't it obey a linear trend? This rudimentary question establishes the primary motives for injecting water or gas into the reservoir during an EOR process. The mass conservation equation indicates that the amount of injection must be equal to the amount of production but it does not say anything about the increment in the rate of production when producer injecting pressure is constant not its rate. For answering this question, we must ask and answer similar questions like what happens if the pressure of producer is remained constant. It is sure that if the rate of producer was constant we would have expected a constant oil production but when the pressure is the controlling factor, what happens is that the total compressibility of the reservoir determines how much it should expand or contract in order to have more or less volume for the injected water; because of that we don't expect a linear trend in oil production rate increasing and decreasing. The decreasing and increasing in the oil production are clearly related to the amount of oil in the reservoir. As the saturation of water increases, the mobility of it also increases so we expect more and more water production gradient (increase in the rate of water production) but notice that although water mobility increases but the rate of water and oil production doesn't necessarily remains constant because the pressure of the producer is

constant not its rate. As the time elapse the reservoir pressure becomes more and more uniform. Therefore the primary force for thrusting water injection i.e. pressure gradient decreases so we expect that water production rate to decrease not to increase. It is very important to note that this is not something that always happen, here the viscosity and formation volume factor of both and oil are assumed to be very similar. So the water/oil slope becomes constant after a while. In another word, the rate of decreasing in oil production will be compensated by water production. Before breakthrough the oil production rate is constant so we expect the recovery factor (or cumulative produced oil) to show a liner trend but after breakthrough the oil production ratio falls down, so we expect the recovery factor curve gradient (or cumulative produced oil) to decrease.

3 Three-dimensional two-phase case

3.1 Reservoir Description

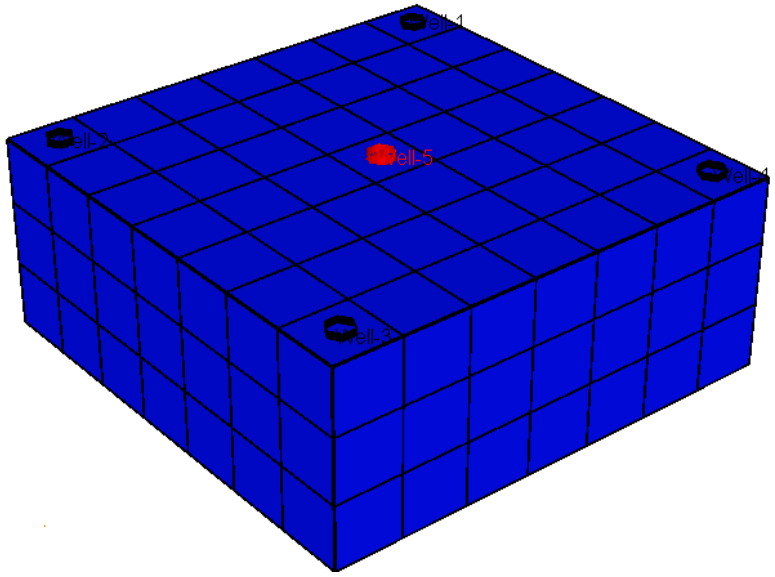

Figure 13: Schematic of the considered reservoir model

A 3D inverse five spot model consisting of 4 producers on the corners of the reservoir and 1 injector in the center of the reservoir is considered (Figure 13). Other characteristics of the reservoir are summarized in below table. The model is assumed to be homogenous and symmetric and the results of only one of the wells are presented below. No-flow condition is considered on the peripheral boundaries of the reservoir.

Reservoir water saturation	Reservoir height	Reservoir width	Reservoir Length	Initial reservoir pressure
0.25	30 ft	200 ft	200 ft	3000 psi

Oil Viscosity	Water Viscosity	Oil Density	Water Density

3 cp	1 cp	45 lbm/ft^3	60 lbm/ft^3

Compressibility factor	Production well pressure	water injection rate
$45e-6\ \frac{1}{psi}$	2500 psi	200 bbl/day

The permeability of the reservoir is considered to be 10 md and the porosity of the reservoir is 0.3. We inject water at the center of the reservoir with a rate of 200 bbl/day and set the production well bottom hole pressure to 2500 psi. The reservoir is simulated for 400 days with a time step of 1 day. The reservoir is divided into 3 layers along the Z axis, 7 grid blocks along the X and Y axis. The reservoir has the same length and width of 200 ft and reservoir height is considered to be 30 ft. Oil and water viscosity are 1 and 3 cp respectively. In this problem, the reservoir length and width are considered to be small so that water breakthrough can be observed in fewer time steps.

3.2 Assumptions

1. The formation volume factor of both oil and water are assumed to be constant.
2. The viscosity of both water and oil is considered to be constant.
3. The reservoir is initially filled with oil so the initial Sw is 0.25.
4. The radius of the wells is set to 0.33.

3.3 Results and Discussion

The results of the simulator for oil production rate, water production rate and water cut are compared with CMG software (Figure 14-Figure 19). As these figures indicate, as soon as the water breakthrough starts, oil production rapidly declines and water cut rapidly increases. At the end of the simulation, however, this change in oil and water

production as well as water cut becomes smooth because the change in oil relative permeability curve near S_{or} is very smooth.

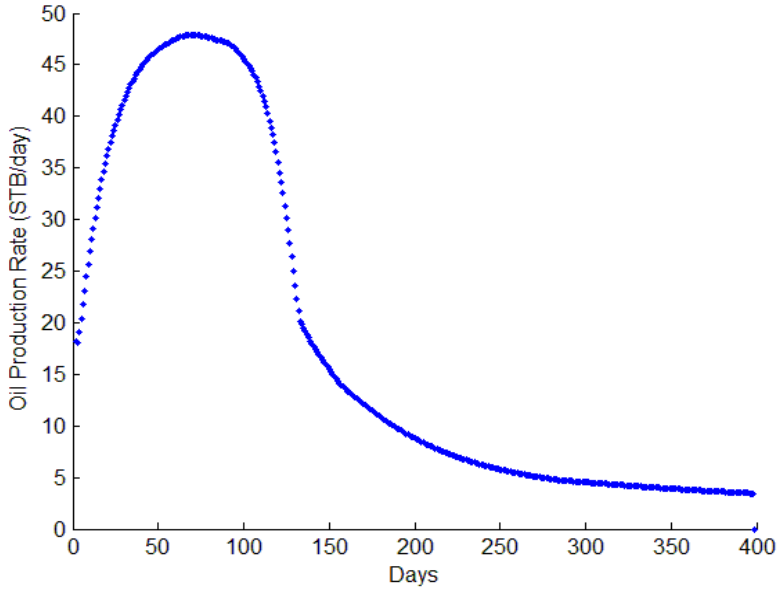

Figure 14: Oil production rate obtained from the simulator

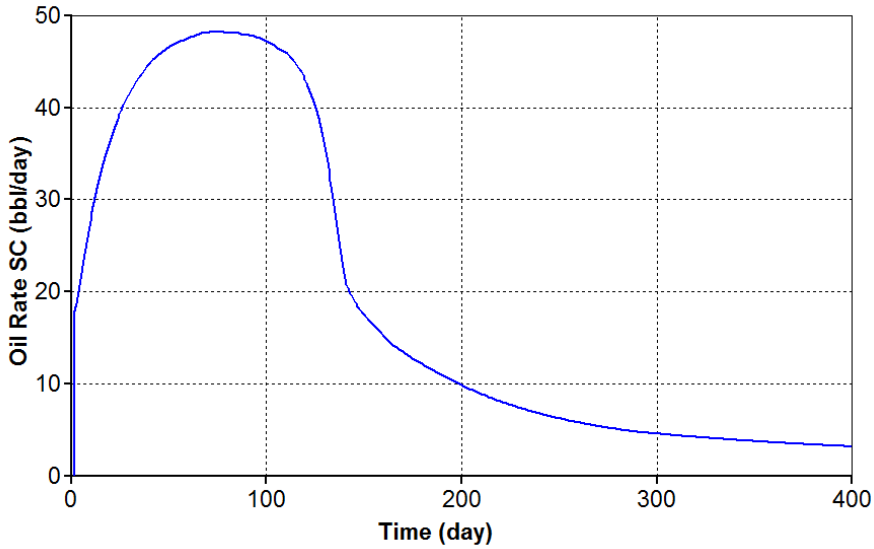

Figure 15: Oil production rate obtained from CMG software

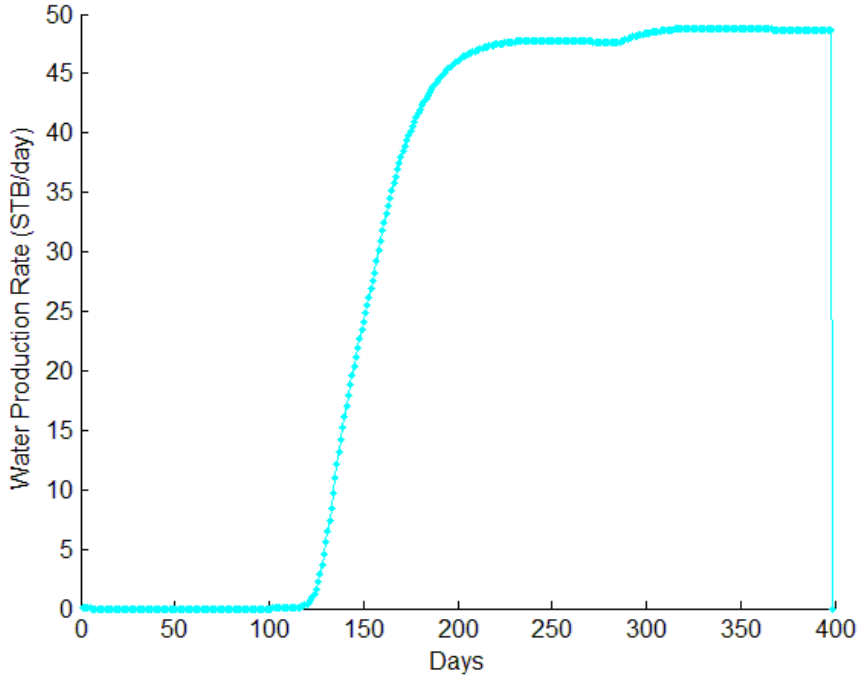

Figure 16: Water Production rate from the simulator

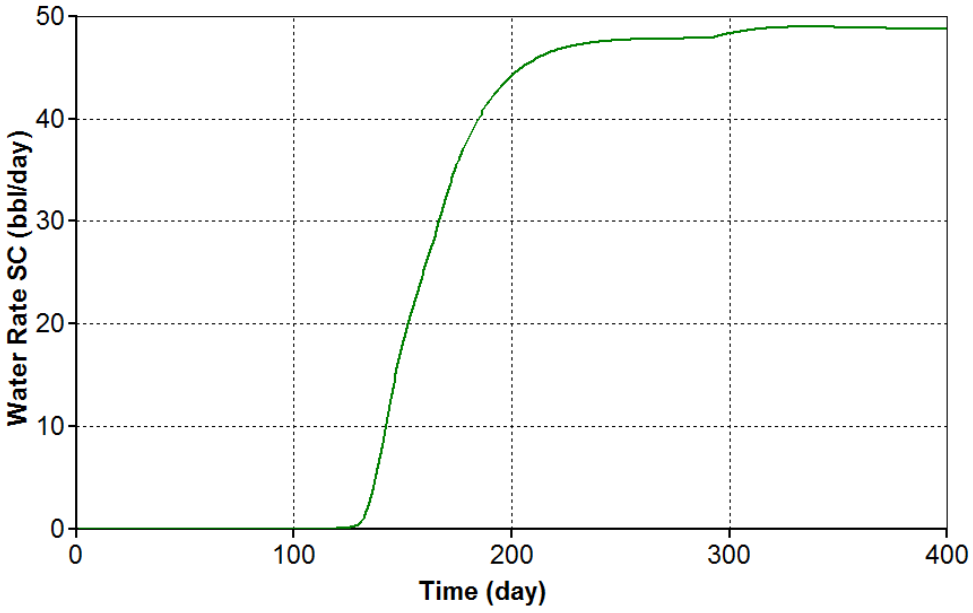

Figure 17: Water production rate from CMG

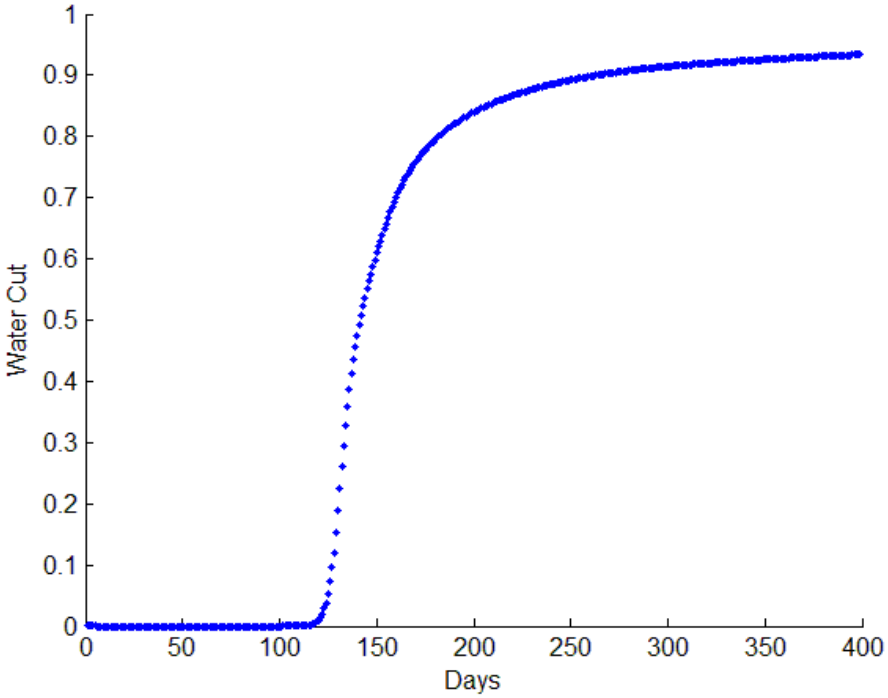

Figure 18: Water cut from well 1 obtained from the simulator

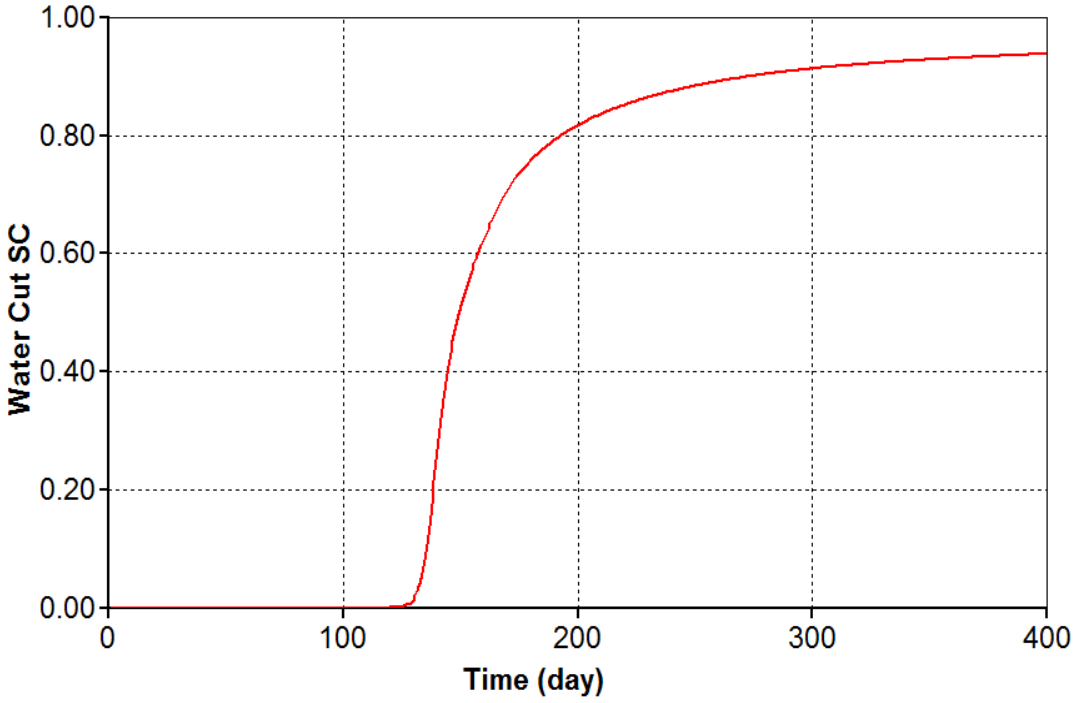

Figure 19: Water cut for well 1 obtained from CMG

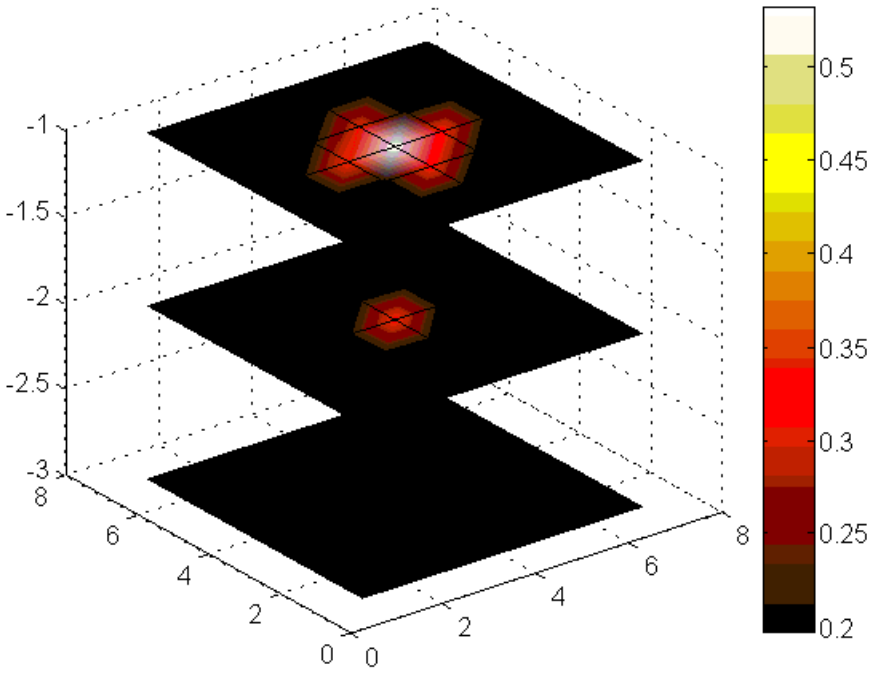

Figure 20: Water saturation distribution after 90 days

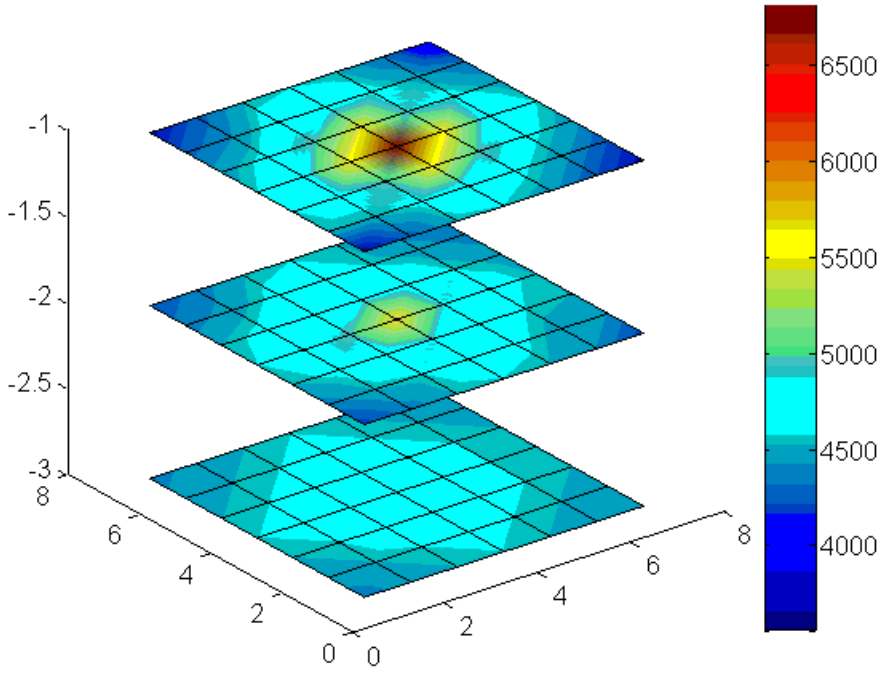

Figure 21: oil pressure distribution after 90 days

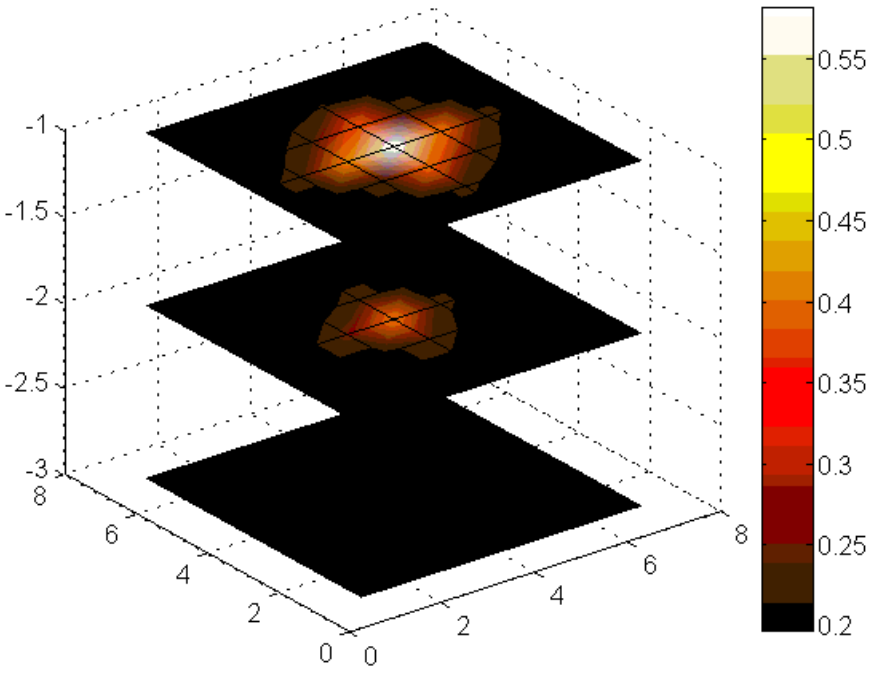

Figure 22: Water saturation distribution after 150 days

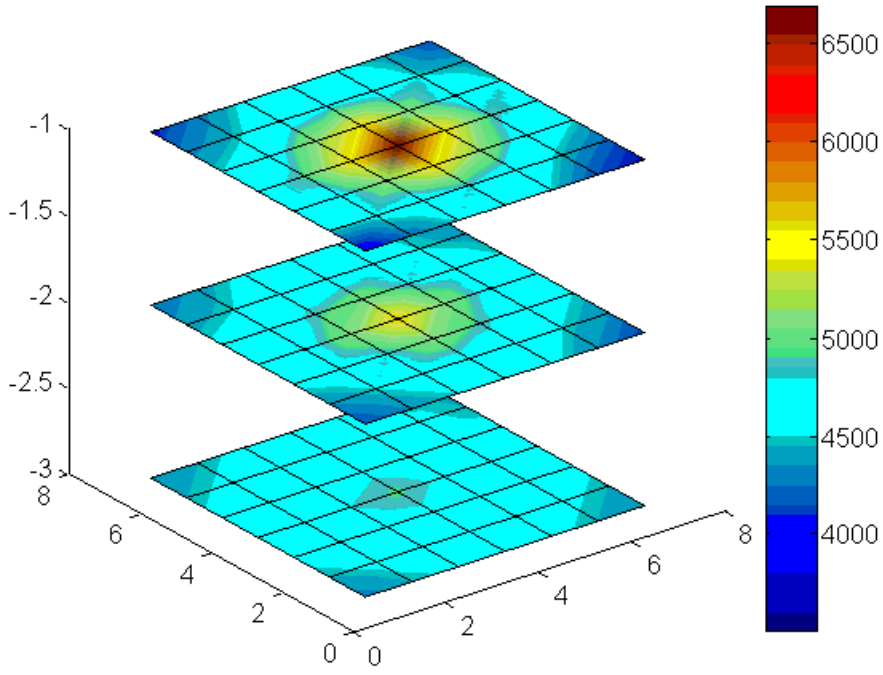

Figure 23: oil pressure distribution after 150 days

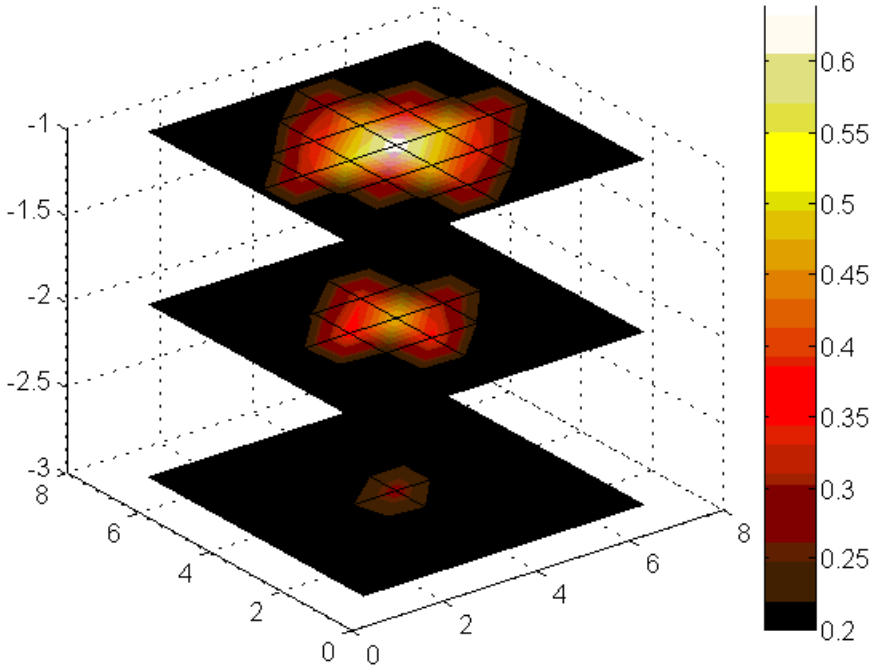

Figure 24: Water saturation distribution after 300 days

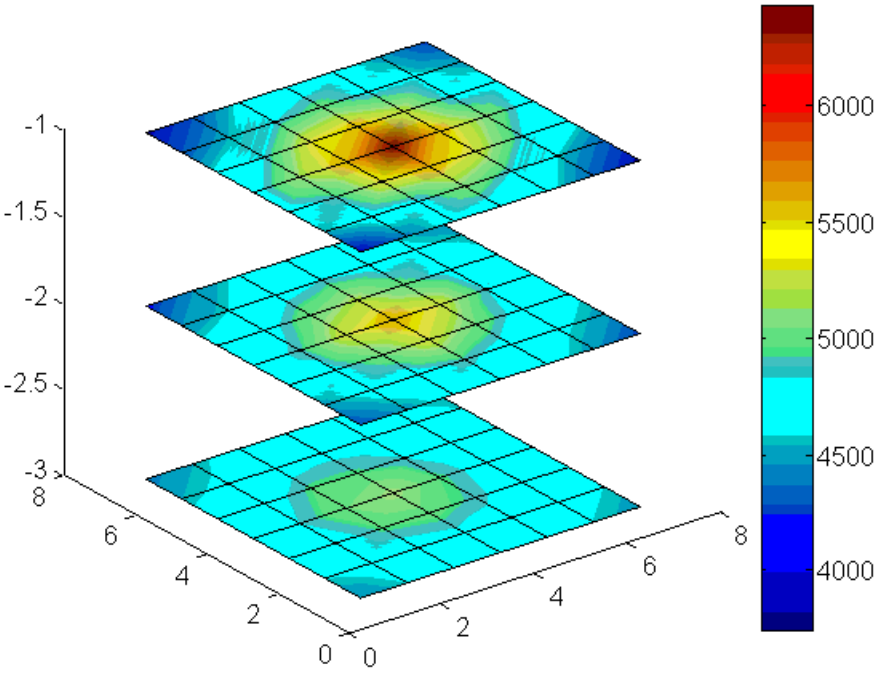

Figure 25: oil pressure distribution after 300 days

4 Pressure Transient Analysis

4.1 Considered Problem:

A 2D square oil reservoir (Figure 26) is considered with one production well at the center of the rectangle. 20 grid cells are considered in the X direction and 20 grid cells in the Y direction. The length and width of the reservoir is 200 ft and the thickness is considered to be 30 ft. The true value of the permeability is 50 for all the grid blocks. The production is 2000 bbl/day. The porosity is considered to be 0.22 and the total compressibility is 45e-6. Initial pressure of the reservoir is 3000 psi. It is assumed that we don't know the permeability of the reservoir and we are interested to calculate it based on the pressure data that we can get from the well by performing a draw down and subsequently a buildup test.

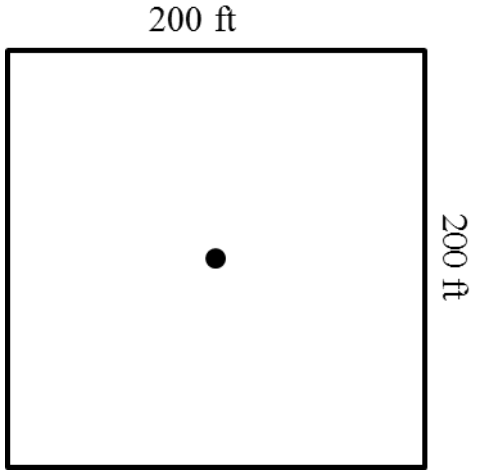

Figure 26: Schematic of the considered problem

The formulation for pressure transient analysis of a cylindrical well is:

$$\Delta p = 162.6\frac{q\mu B}{kh}\left[\log(\Delta t) + \log\left(\frac{k}{\phi\mu C_t r_w^2}\right) - 3.23 + 0.87\,S\right] \qquad \text{Eq. 50}$$

4.2 Draw down test

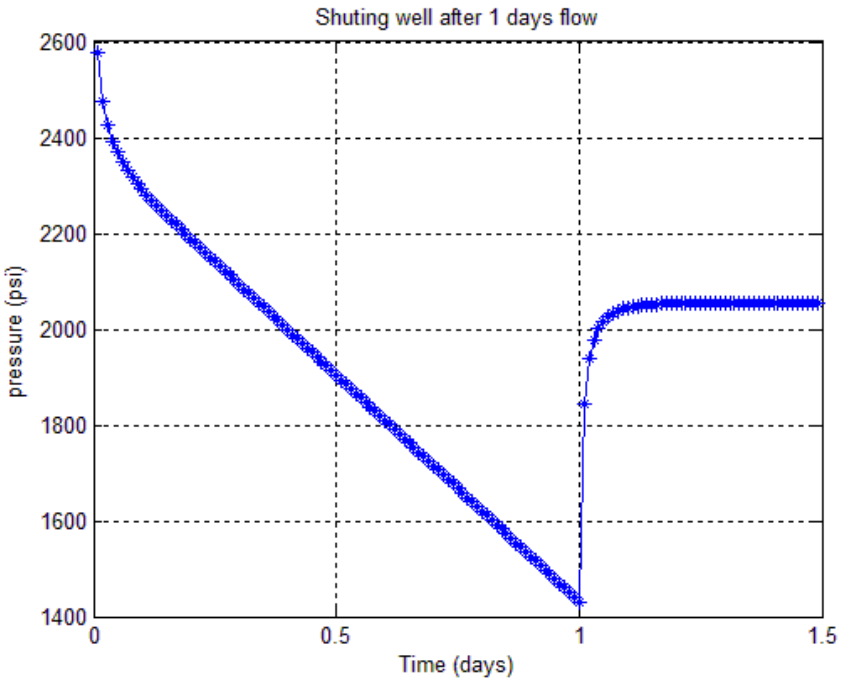

Figure 27: Pressure of the well vs. Time

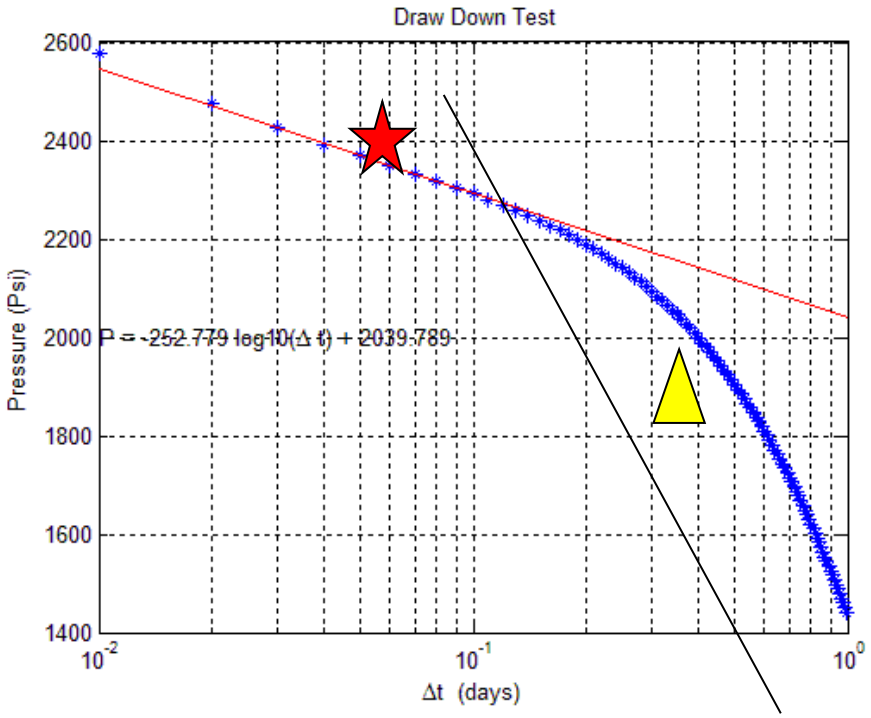

Figure 28: MDH plot for drawdown test

The draw down test is sketched in a semi-log plot (MDH method). This image demonstrates that a straight line for the first period of draw down test can be drawn very exactly. The question that might arise here is that there is more than one straight line which can be drawn between the points. However, the triangle straight line is not a correct line since the curvature between the star and the triangle line shows the collusion of pressure transient into the boundary. The triangle straight line represents the boundary effect. The boundary is closed and we expect such a curvature behavior from well test analysis. The star line however reflects the pressure draw down before the boundary effect and can be used for measuring the permeability around the injection well. Since there is no skin, the first points should be used for measuring the slope of the straight line. The slope is 252.779 psi/cycle, therefore the permeability is measured:

$$k = 162.6\frac{q\mu B}{mh} = 162.6\frac{2000 * 1 * 1}{252.779 * 30} = 42.8833 \qquad \text{Eq. 51}$$

4.3 Build up test

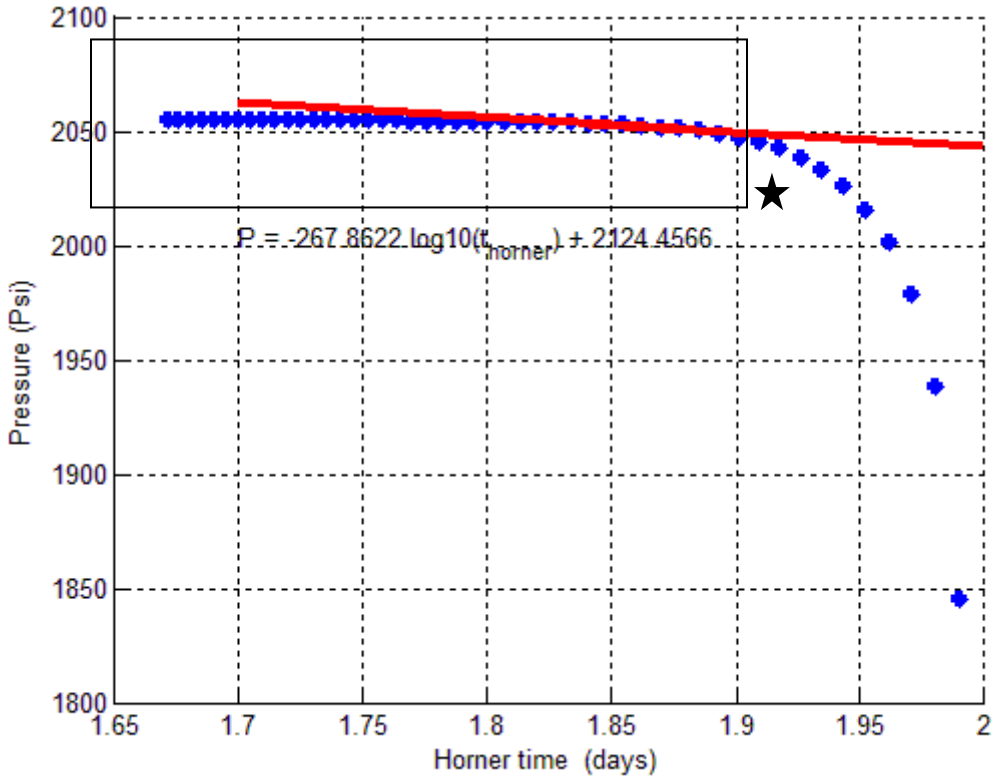

Figure 29: Horner plot for pressure build up test

The buildup of the previous image is sketched in semi-log coordinates (the value of the time is in logarithmic). The time is set to be Horner time. In the Cartesian plot the build up test showed a very steep behavior around the shutting time. This steep characteristic is transformed to a very flat line in the semi-log coordinates when the time equivalent is set to Horner time. However the line which consists of more points can be selected as the straight line and is used for measuring the permeability. Finding the best straight line

which consists of more points is very crucial and requires careful efforts. The rectangular shows the domain where possible straight line can be drawn but notice that not all of them will give a correct slope, a program has been written in MATLAB to determine the best possible lines but since the place of this line is uncertain (due to steep behavior of the pressure change at the beginning of the buildup test); this program is unreliable and may fail to determine the exact position of the straight line. Optically determining the place of the straight line however, proved to be the best method. The star shows the place where the boundary effect is felt in the well. The straight line is drawn in a place where it consists of more points.

$$k = 162.6\frac{q\mu B}{mh} = 162.6\frac{2000 * 1 * 1}{267.8622 * 30} = 40.4686 \qquad \text{Eq. 52}$$

4.4 Sensitivity analysis to improve the permeability

Time step, shut in time and number of grid blocks are selected for sensitivity analysis and in order to calculate permeability more accurately.

Draw Down Test (actual permeability =50)		
Gird Blocks	m (psi/cycle)	k(md)
20	252.779	42.8833
26	251.3118	43.1337
30	250.7964	43.2223
36	250.3277	43.3032
40	250.1273	43.3379

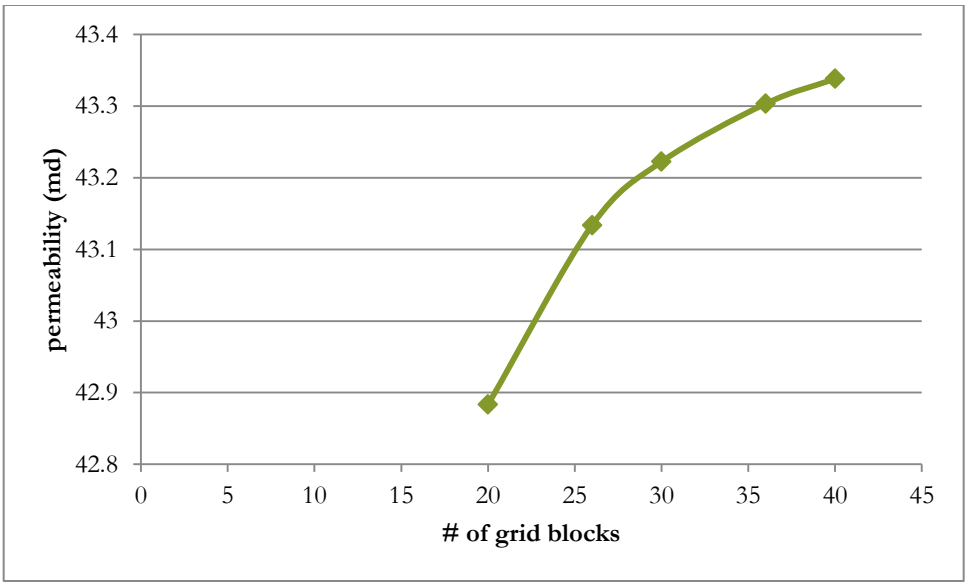

Figure 30: The effect of changing mesh grids on the permeability accuracy in draw down test (true k= 50 md)

The result of draw down test for various mesh grids shows that an increase in number of grid blocks improves the measured permeability, this result makes sense since more grid blocks means more pressure calculation on the two dimensional plane. A reduction in pressure between grid blocks means that the slope of the semi-log plot decreases. This eventually translates into a more accurate permeability. This increase in the permeability increases computational time. On the other hand, the rate of improvement in permeability accuracy decreases as the number of the grids increases (Figure 30).

Build Up Test		
Gird Blocks	m (psi/cycle)	k(md)
20	267.822	40.4746
26	251.2915	43.1372
30	245.3211	44.1870

36	239.8189	45.2008
40	237.4439	45.6529

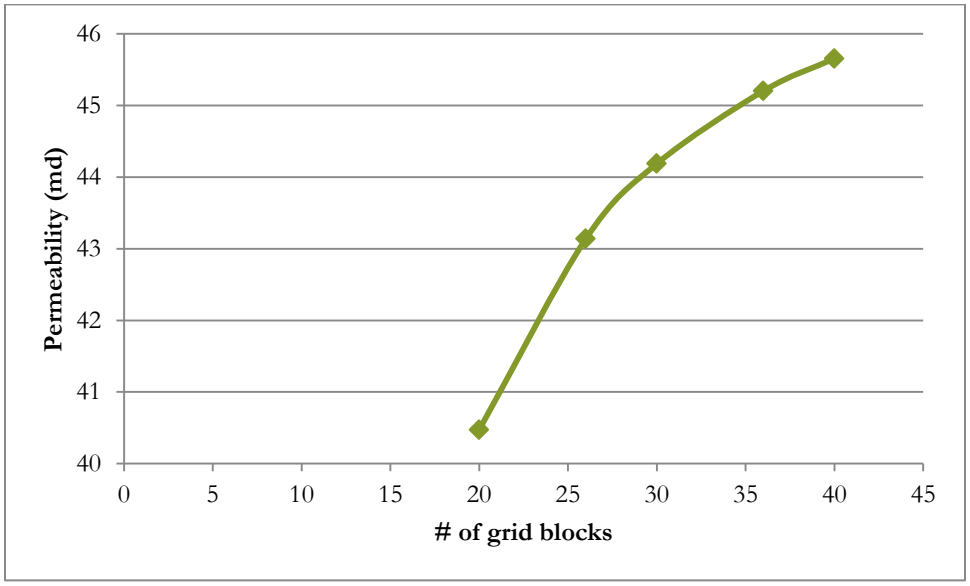

Figure 31: Effect of changing mesh grids on the permeability accuracy in buildup test (true value =50)

The same analysis for buildup test results in similar observations. The results for the buildup test for various mesh grids shows that an increase in grid blocks improves the measured permeability (Figure 31). As it was explained, getting different slopes for the straight line at the beginning of shut in time and optically choosing the best line which consists of more points makes the analysis difficult. But the prevailing trend in the data describes that more grid blocks returns more accurate permeability. The same reasons, as in the draw down test, can be applied here. The result of build up test may appear more promising than that of draw down test; however the slope of the straight line in the draw down test is chosen programmatically rather than optically. This gives more credit to the slope and permeability that has been measured by builds up test.

4.4.1 Effect of shut-in time

Figure 32 shows that the flowing time has no effect on calculating permeability. This result makes sense and is expected because the slope is completely independent of flowing time. The first points of the flowing time will participate in measuring permeability which makes the permeability insensitive to the flowing time.

Draw Down Test		
Shut in Time (days)	m (psi/cycle)	k (md)
1/5	252.779	42.8833
1/3	252.779	42.8833
0.5	252.779	42.8833
1	252.779	42.8833

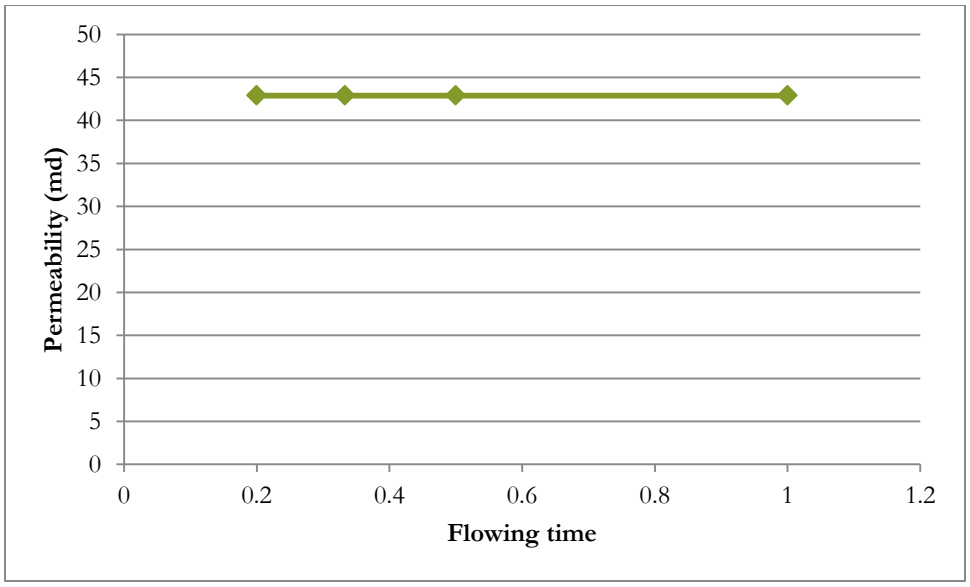

Figure 32: The effect of changing flowing time (before shut in) on the permeability

4.4.2 Effect of time step

Decreasing time steps yields more accurate permeability; however more reduction in time steps after some specific point may have contrary results. The increase in permeability by decreasing the time step is expected since the pressure calculation in the production grid becomes more accurate. More accurate pressure in the production grid means less pressure and therefore a drop in the slope and increase in calculated permeability. Therefore in order to have a more accurate permeability we can choose a less time step.

Draw Down Test		
Time Steps (days)	m (psi/cycle)	k (md)
1/200	245.1511	44.21763
1/150	245.3796	44.17645
1/120	247.9761	43.71389
1/110	249.8947	43.37827
1/100	252.779	42.88331
1/90	257.126	42.15832
1/80	263.7446	41.10037

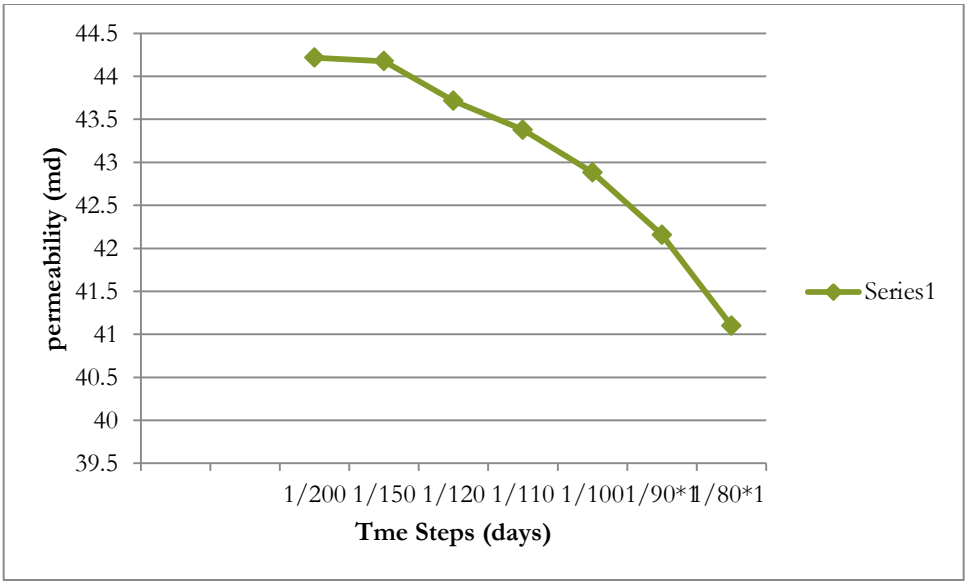

Figure 33: the effect of changing time steps on permeability

4.5 Improved permeability for the Draw down test

If we set the number of mesh grids to 40 and the time steps to 1/200, the result gets better. However, this requires more computational time. The time for such calculation is estimated to be about 2 minutes.

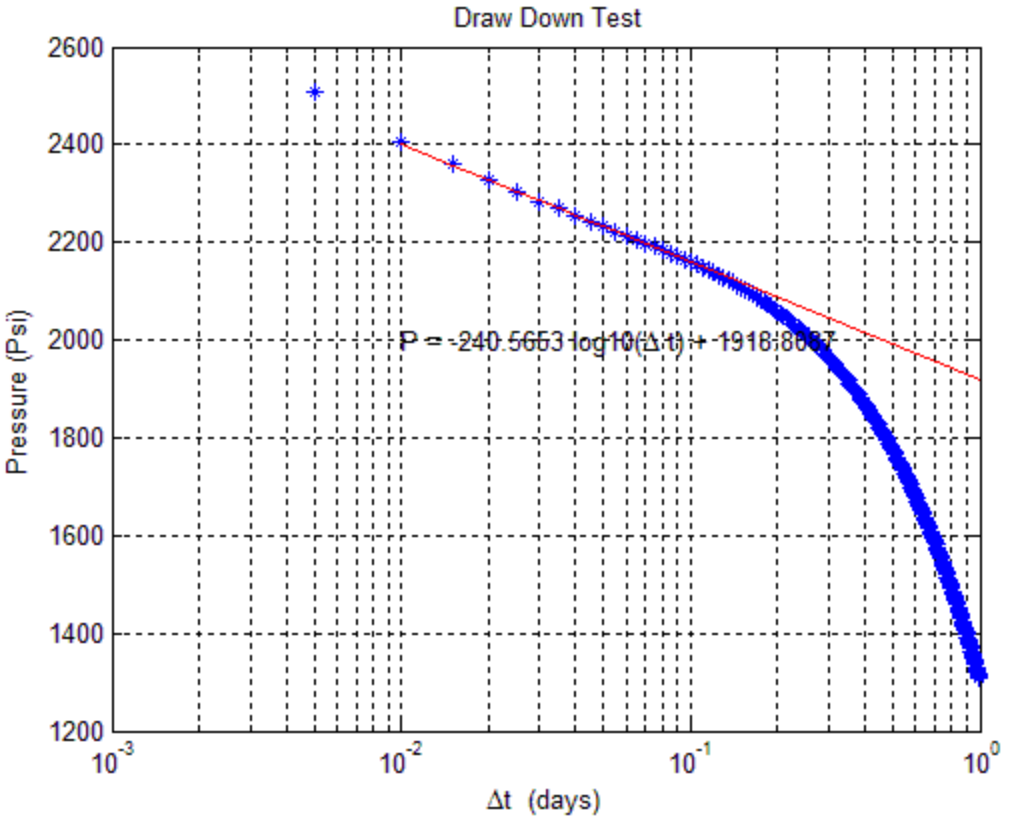

Figure 34: The result for 40 mesh grids and 1/200 time steps.

So the permeability can be calculated:

$$k = 162.6\frac{q\mu B}{mh} = 162.6\frac{2000 * 1 * 1}{240.5663 * 30} = 45.0603 \qquad \text{Eq. 53}$$